Applied Composite Materials (2020) 27:337–355
https://doi.org/10.1007/s10443-020-09819-1

Virtual Description of Non-Crimp Fabrics at the Scale of Filaments Including Orientation Variability in the Fibrous Layers

David Colin [1] · Sylvain Bel [2] · Thorsten Hans [1] · Mathias Hartmann [1,3] · Klaus Drechsler [1]

Received: 12 March 2020 / Accepted: 5 June 2020 / Published online: 6 July 2020

Abstract
A numerical description of dry non-crimp fabrics is proposed at the scale of the filaments using a commercially available finite element software package. Deviations in the filament orientation of the fibrous layer is a dominant factor in the occurrence of local defects, which influences the mechanical response of the textile. Therefore, the introduction of variability in the orientation distribution is proposed in this paper. This approach enables to capture the entanglement of the filaments and models all interaction mechanisms. A stepwise generation of the numerical non-crimp fabric is proposed considering the main manufacturing steps to reproduce the local defects in the fibrous mat appropriately. Averaged periodic boundary conditions are developed ensuring an overall periodicity of the model while allowing reorientation at the scale of the filaments. Two various non-crimp fabrics are investigated and modelled. The distribution of the filaments in the simulation results correlate well with measurements of the filament orientation performed on the textiles. Moreover, a detailed comparison of the local defects shows a good agreement with measurements on the specimens. The presented approach can be used to generate geometries for subsequent virtual characterization.

Keywords Textiles · Defects · Finite element analysis (FEA) · Non-crimp fabrics · Digital chain elements

✉ David Colin
david.colin@tum.de

[1] Chair of Carbon Composites, TUM Department of Aerospace and Geodesy, Technical University of Munich, Boltzmannstraße 15, 85748 Garching, Germany

[2] LMC2, Université Lyon 1, 82 Blvd. Niels Bohr, Domaine Science DOUA, 69622 Villeurbanne Cedex, France

[3] Technologie Campus Hutthurm, Technische Hochschule Deggendorf, Hochleiten 1, 94116 Hutthurm, Germany

1 Introduction

The use of Carbon Fiber Reinforced Plastic (CFRP) in structural applications has been increasing constantly over the last decades due to their unique lightweight potential. Besides the utilization in aerospace components, CFRP has been established for automotive structural parts, which requires high production rates and, therefore, challenges the traditional manufacturing techniques in terms of quantity and reproducibility. Remedy is the use of dry carbon reinforcements in automated processes (e.g. resin transfer molding or wet compression molding) enabling suitable short cycle times. Moreover, the quest for stiffer and lighter parts requires adapted reinforcement textiles. Multilayer multiaxial Non-Crimp Fabrics (NCFs) are very attractive because they are constituted of single or multiple unidirectional layers stitched together with a binding yarn, which enables to tailor the stiffness and strength of the laminate. Compared to woven fabrics, the out-of-plane undulation of the filaments is widely reduced, leading to superior mechanical performance compared to woven fabrics, while offering comparative good handling capabilities [1]. However, the introduction of the binding yarn induces complex deformation mechanisms during the draping of flat preforms into the desired part shape. As introduced by Creech and Pickett [2], the deformation mechanisms of dry NCFs during preforming steps result from various interactions, which can be gathered into three groups: the inter-filament, the inter-stitch [3, 4] and the stitch-to-filament interactions. The relative importance of each interaction mechanism varies for each individual NCF configuration, resulting in different deformation behavior of the textile [5]. Two different NCFs, which are representative of the high variety of textile configurations, are illustrated in Fig. 1: a biaxial 0°/90° tricot-chain stitched NCF from SGL KÜMPERS® and a biaxial ±45° tricot stitched NCF from SGL Group®. Their respective characteristics are listed in Table 1. In the following, they are referred to as the "0°/90° NCF" and "±45° NCF", respectively.

These two NCFs are representative of the differences between the NCF configurations, which lead to different deformation behaviors. Firstly, the orientation of the layers influences the shear behavior: ±45° biaxial NCFs show a potential asymmetric shear behavior due to the stiffness of the stitching yarn introduced in the bias direction [3, 6]. Moreover, the stitching pattern may influence the deformation mechanisms of the textile considerably [5, 7, 8]. Furthermore, studies focusing on the alignment of the filament [9, 10] have shown considerable deviations from the global direction, which might influence the inter-filament interactions and therefore the overall behavior of the NCF. Moreover, the fibrous layer exhibit local defects at the stitching points, deviating locally the filament path from the theoretical layer orientation. These defects can be a continuous gap that connects many stitching points (referred to as "channels") or local fish-eye distortions, commonly defined as "cracks" [11]. The type and size of these defects may also have an influence on the interaction mechanisms, modifying the mechanical behavior of the textile. A detailed identification of these defects on the 0°/90° and ±45° NCFs is proposed in section 3.

The development of numerical approaches to model the complex behavior of NCFs represents an attractive method to understand and predict their deformation behavior. Predictive models can be implemented – as proposed by Harrison et al. [12] – in order to reduce costly and time-intensive material characterization. Moreover, they enable to study the influence of manufacturing process parameters in a wide range. For example, the influence of the stitching length, stitching gauge or stitching pattern on the deformation behavior of the textile can be investigated. The overall goal of the present work is the

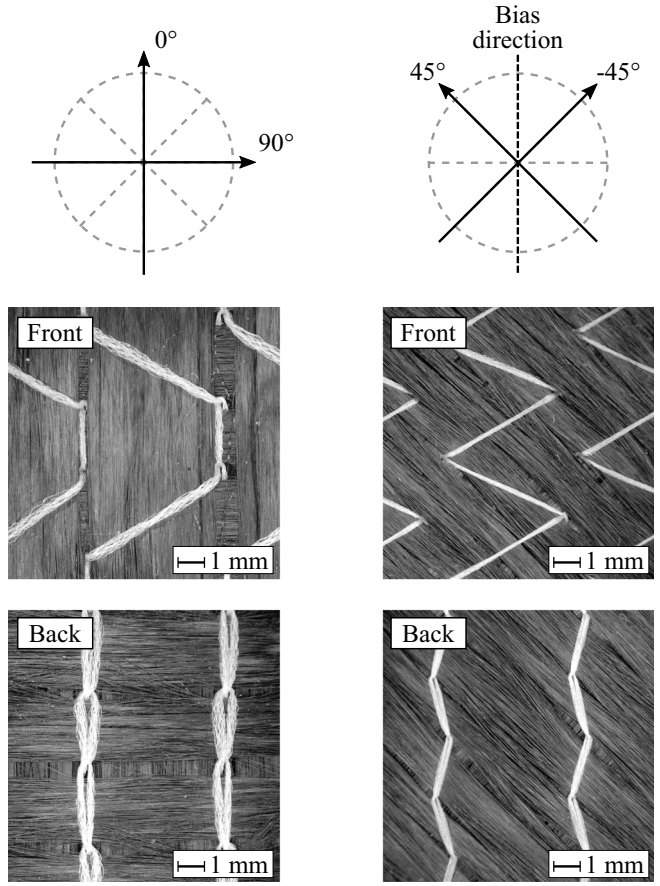

(a) Biaxial 0°/90° NCF tricot-pillar pattern

(b) Biaxial ±45° NCF tricot pattern

Fig. 1 Example of two representative biaxial NCF configurations with their respective layer orientations

development of a model capable of numerically describing the filament architecture and the interaction mechanisms of NCF that can be used in further simulation steps to predict the mechanical behavior of a large range of NCF configurations.

2 Background

2.1 Numerical Modelling of Non-crimp Fabrics

Various simulation strategies to model dry NCFs are reported in the literature. Three modelling scales can be identified depending on their discretization level and will be detailed in this paper for biaxial NCFs. First, models implemented at the macroscopic scale homogenize the properties of the reinforcement with a continuum description and account for various process parameters [7, 13–15]. Those simulations can predict the occurrence of out-of-plane wrinkles or filament reorientation if properly calibrated. However, important deformation mechanisms

Table 1 Material data from the non-crimp fabrics considered in this study

	0°/90° NCF	±45° NCF
Description	Biaxial carbon fabric	Biaxial carbon fabric
Total areal density [g/m^2]	300	308
Orientation of the plies [°]	0°/90°	+45°/–45°
Filament material	SGL Sigrafil CT24–4.8/240	SGL Sigrafil CT50–4.4/255
Filament count in tow [–]	24 K	50 K
Filament tensile modulus [GPa]	240	255
Filament density [g/cm^3]	1.81	1.78
Stitching pattern	Tricot-chain	Tricot
Stitch gauge [needles per inch]	5	5
Stitch length [mm]	2.8	2.2
Stitching yarn	PES 7.6 tex	PES 5.0 tex

listed above are not modeled (e.g. relative sliding between the tow and stitches) limiting the predictive capabilities. Moreover, time-consuming materials characterization is required to generate the appropriate inputs. A refined model accounting for the influence of the stitching yarn on the deformation modes has been recently proposed by Steer et al. [16] in which the deformation energy induced by the deformation of the stitching threads and the inter-stitch interactions is computed analytically. While this approach can predict the influence of the stitching pattern and some manufacturing parameters on the overall mechanical response, local defects or stitch-to-filament interactions and their influence on the deformation behavior cannot be considered. On the other hand, Bel et al. [17] proposed an approach discretizing the NCF with one continuum element per layer and modelling the stitching yarns separately. This enables to account for inter-layer interactions and the interaction of the layers with the stitching yarn. Thus, the tow-sliding can be simulated. In the second modelling scale, models that describe the meso-structure of the reinforcement can predict the occurrence of gaps or in-plane waviness if the layers are discretized in tows [2, 18–21]. Despite an enhanced description of the deformation mechanisms, a homogenization of the tow behavior is still necessary to gain results on part level within an acceptable calculation time span. This makes this approach inflexible, as adaptations are necessary for any new NCF configuration even with only slight changes (e.g. other stitch length). Moreover, the definition of tows and their discretization remains a challenge for NCFs with ±45° layer orientation if the ratio between the stitching gauge and length are not appropriately selected. Finally, descriptions of the textile at the scale of filaments or group of filaments can be proposed, also referred to as discrete modelling or multifilament approaches [19, 22, 23]. This level of refinement describes the relative motion between the filaments. The predictive capabilities are improved, since the homogenization is reduced to a lower amount of real filaments and all relevant interaction mechanisms are considered. Such approaches have been mainly reported for the simulation of textiles with well-defined tows. Applied to NCF, discrete modelling enables to account for the inter-filament, the inter-stitch and the stitch-to-filament interactions. Moreover, the local defects listed in section 1 (cracks, channels) can be reproduced.

2.2 Discrete Modelling of Fibrous Materials

First discrete modelling approaches of dry textiles using Digital Chain Elements (DCE) have been presented by Zhou et al. [24]. They consist in chains of rod-elements connected with

frictionless pins. The frictionless hinges between the rod-elements ensure a free rotation at the connecting nodes. It is assumed that the forces induced by the bending deformation of the single filaments are negligible compared to the forces induced by the interactions within the textile. The modelling technique has been used to study the geometry of woven fabrics and braids through a detailed stepwise manufacturing process, leading to high computation time. More recently, Huang et al. [25] proposed to start from an idealized geometry of the weaving pattern and applied tension to the yarns to generate the woven geometry. This approach enables to reduce the computation time while reaching a realistic model of the microscopic geometry. However, this method is limited to textile architectures with a high level of interlacing, such as 3D-woven fabrics. In addition, Durville proposed the modelling of reinforcement textiles at refined scale. In [26] many filaments are merged in a single element. Using an enriched kinematic beam model, it enables to account for the bending stiffness and the deformation of the cross-section of filament bundles. This approach was applied to woven fabrics and rovings for braided textiles [27] in order to study the shear and compression behavior, respectively. The approach presented by Durville is based on a progressive resolution of interpenetration of the bundles to generate the textile geometries. The calculation method relies on an implicit integration scheme, which requires intensive development efforts of the contact algorithms to reach a reasonable convergence rate with commercial FE solvers. A further discrete modelling technique of textiles was proposed by Green et al. to study the compaction behavior of 3D woven preforms using conventional beam elements [28]. However, merging many filaments in one conventional beam element would lead to an overestimation of the bending stiffness. To tackle this problem, Green et al. used an elastic-plastic model in order to reduce the bending stiffness of the bundles when a deflection threshold is exceeded. The simulation results correlated well with computed tomography scans even though they concluded that this approach is not able to reproduce the forces in the woven fabric accurately when deformed. Moreover, the results are sensitive to the yield strength used to reduce the bending stiffness of the chains.

As reported above, discrete modelling approaches have been mostly applied to fibrous material with woven or braided architectures. Thompson et al. [23] proposed a workflow to predict the mesoscopic geometry of the tows of a biaxial 0°/90° NCF with the use of the multifilament approach. The virtual description of the NCF was generated starting from an idealized periodic alignment of the chains with predefined gaps between the tows. A negative temperature was subsequently applied to the stitching yarn to reproduce the manufacturing process. To the author's knowledge, the study presented by Thompson et al. in [23] is the only work published so far focusing on the application of discrete modelling to NCFs. Nevertheless, their approach is limited to NCFs constituted of 0° and 90°-layers, in which well-defined tows can be identified. Also, the assumption of periodic and perfect alignment of the chains do not account for local deviations of the chain orientation from the idealized path. Therefore, it fails to model the occurrence of various local defects and, thus, might underestimate the interactions in the textile. Further development is necessary to apply the discrete modelling approach on NCFs with various layer orientations that do not exhibit a purely periodic structure at the level of the filaments, as it is generally the case for ±45°-layers. Moreover, local deviation of the filament orientation from the theoretical orientation is essential for the reproduction of the local defects in the fibrous.

2.3 Objective

The present study proposes a new method to apply the discrete modelling approach to a large panel of NCFs in which not only well-defined yarns are observed. The variability of the

filament orientation is introduced resulting in fibrous layers that account for the entanglement of the filaments and the local defects in the fibrous mat. The three-dimensional generation of the numerical model is based on the manufacturing parameters of the stitching machine and on the variability in the fibrous mat before the stitching process instead of usual geometrical inputs generated by micrographs or computed-tomography. Moreover, the proposed approach enables the consideration of any layer orientation and stitching pattern. First, an experimental quantification of the filament orientation distribution and local defects is proposed. Then, the approach to model the fibrous structure of the NCF including the variability of the filament orientation is detailed and applied to the ±45° and 0°/90° NCF configurations. Finally, a detailed comparison of the numerical NCFs with real samples is presented. It shows a good correlation of the resulting filament orientation distribution and local defects generated in the fibrous layers. The numerical description of the NCF based on this approach can be used in further mechanical analysis to investigate its deformation behavior.

3 Measurement of the Distributions of the Filament Orientation and Defect Formation in NCFs

3.1 Filament Orientation

A characterization of the distribution of the filament direction was first performed to quantify the actual deviation of the filaments from the theoretical path and to study local defects in various NCF configurations. The orientation measurements were performed using an optical F-Scan Sensor from Profactor GmbH [29] on both sides of the 0°/90° and ±45° NCFs introduced in section 1. In this way, each layer can be observed separately. The results are depicted in Fig. 2, showing the local deviation of the filament orientation from the theoretical layer orientation. The stitching yarn and the underlying fibrous layers are excluded from the measurement in order to consider each layer separately. This also emphasizes the local defects in the fibrous layers. In a 0°/90° NCF, the filaments should theoretically align with the stitching points, resulting in channels only. Nevertheless, it can be observed in Fig. 2(a) that a few filaments of the 0°-layers are crossing the channels between the stitching points and that cracks are generated in the 90°-layer (see Fig. 2(b)). Therefore, the types of defects depend not only on the orientation of the layers with regard to the stitching points but also on the distribution of the filaments resulting from the spreading process (i.e. the waviness and fiber misalignment present in the fibrous layers prior to the stitching process). Moreover, cracks are observed in both layers of the ±45° NCF, as illustrated in Fig. 2(c) and Fig. 2(d). The distributions of the filament orientation are illustrated in Fig. 3 using the nominal layer orientation as a reference. While comparable distributions are measured on both +45° and −45°-layers, significant differences can be observed for the 0°/90° NCF. The 0°-layer exhibit a narrower distribution than the 90°-layer, which correlates well with the previous observation of the local defects. Therefore, it is identified that the types of defects are closely related to the orientation distribution of the fibrous layers. Moreover, it is expected that a higher spread in the distribution of the filament orientation leads to a higher degree of entanglement of the filaments (i.e. inter-filament interactions) and to an increased interaction with the stitching yarn. As a result, it is expected that the filament orientation distribution influences the overall deformation mechanisms of the textile and must be accurately modelled in the numerical description of the textile.

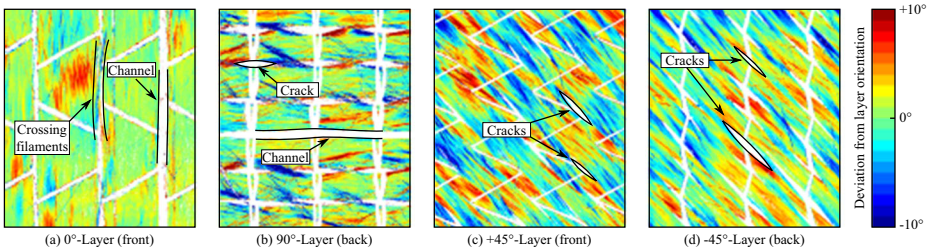

Fig. 2 Local deviation of the filament orientation from the theoretical layer orientation on the 0°/90° NCF (a), (b) and ±45° NCF (c), (d) with identification of the local defects

3.2 Defect Size

The size of the local defects was measured in each layer with a minimum of 40 measurement per layer. In the 0°-layer of the 0°/90° NCF, the width of the channels was evaluated in the middle of the tricot segments. Due to the presence of the stitching yarn, the width of the cracks in the 90°-layer could not be evaluated accurately. Therefore, only the crack length of the 90°-layer was measured. In the ±45° NCF, cracks are observed in both layers. As showed in Fig. 2, the fibrous mat of the +45°-layer covers the stitching yarns at some locations and prevent the measurement of any defect. This happened in 35% of the selected locations. In this case, further points were selected to achieve a minimum of 40 measurements in each layer. The results of the defect measurement are listed in Table 2. The local defect in the fibrous layers vary considerably in width and length. In addition, the angular tilt of the loops was investigated in the −45°-layer to quantify their deviation from the machine direction. A mean angle of 14.9° with a standard deviation of 1.3° was determined. These observations correlate well with the results reported by Lomov et al. in [11], where the cracks induced in various NCFs and the angular tilt of the stitching loops were characterized extensively.

These experimental observations will be used to validate the numerical description of the NCFs developed in section 4.

4 Generation of the "as-Manufactured" Geometry

4.1 Numerical Description of the Filaments

In the present work, digital chains using truss elements have been implemented in the commercially available finite element software package Abaqus/Explicit. Using this type of elements, the bending stiffness of the chains is neglected. Within this approach, the forces result from the axial deformation of the truss elements and from friction between the chains. A conventional Coulomb friction law is used to calculate the frictional forces. Moreover, it is expected that the deformation behavior of the textile in thickness direction mainly derives from the rearrangement and relative displacement of the filaments. Since DCE exhibit a constant cross-section, the discretization level of the fibrous mat should be sufficiently refined to reproduce the rearrangement and interaction between the chains accurately. This approach is especially attractive because it reduces the amount of degrees of freedom and requires few inputs.

Table 2 Size of the local defects measured on the NCFs

Designation	Layer	Defect type	Characteristic	Mean value [mm]	Standard deviation [mm]
0°/90° NCF	0°	channels	width	0,50	0,24
0°/90° NCF	90°	cracks	length	2,30	0,70
±45° NCF	45°	cracks	length	3,19	0,81
±45° NCF	45°	cracks	width	0,21	0,09
±45° NCF	−45°	cracks	length	3,58	0,89
±45° NCF	−45°	cracks	width	0,22	0,09

4.2 Generation of the Fibrous Mat

Depending on the manufacturing technics and the layer orientations, uniformly distributed fibrous layers are used during the knitting process to manufacture the NCFs. In this case, the needles do not penetrate the layers between precisely laid tows but pierce the fibrous mat [30, 31]. Therefore, it is proposed to generate fibrous layers homogeneously distributed in order to consider a wide variety of multiaxial NCFs and to reproduce the manufacturing process accurately.

In a first step, the variability of the filament directions is introduced with digital chains initially modelled straight with an angle randomly sampled based on a Gaussian distribution located at the reference layer orientation. Each chain is modeled at a various out-of-plane coordinate to avoid any non-physical interpenetration of the chains. If a chain crosses the border of the modeled volume element, it is projected on the corresponding face on the other side of the volume element (see Fig. 4(a)). Hence, the amount of digital chains is kept constant for any cross section of the modeled fibrous mat. Subsequently, a simulation step using two rigid plates is necessary to compact the chains to the final homogeneous fibrous mat. Thereby, the displacement of the end-nodes of the chains is allowed only in the vertical direction. This simulation step enables an efficient resolution of the potential interpenetration with an explicit solver and leads to the onset of undulation and entanglement of the chains – as illustrated in Fig. 4(b). The compaction step is performed until the distance between the plates reaches a predefined value. Since the thickness of the NCF material in a relaxed state is a priori not known, a coefficient similar to the Fiber Volume Fraction (FVF) is introduced to characterize the packing state of the relaxed material. The thickness t_L of the generated layers after compaction is calculated as follows:

$$t_L = \frac{A}{V_L \cdot \rho_f} \tag{1}$$

where A corresponds to the areal weight of the layers, V_L is the prescribed FVF and ρ_f the density of the filaments. The thickness of the fibrous mat before the stitching is calculated based on an overall FVF of 20%.

In the case of a purely periodic material (i.e. without variability), the chains are directly distributed homogeneously within the volume element with a thickness t_L. Since the stitching process induces local shifting of the filament directions from the reference path, the sampling of the homogeneous fibrous layers cannot directly rely on the measurement presented in Fig. 3. Therefore, various standard deviations are implemented and only the orientation of the chains of the final "as-manufactured" geometry are compared to the

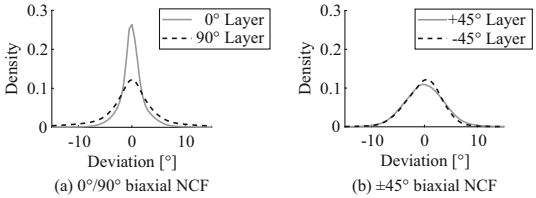

Fig. 3 Probability density of the deviations of the local filament orientation from the theoretical layer orientation

experimental measurements. Figure 5 illustrates the resulting architecture of the fibrous layer for an exemplary 0°-layer without variability an with normally distributed filament orientations featuring standard deviations of 0.3°, 1.0° and 3.0° respectively. It can be observed that the standard deviation significantly influences the interlacing of the chains and confirms the ability of the approach to reproduce the entanglement of filaments.

4.3 Averaged Periodic Boundary Conditions

Due to the high refinement scale of the presented approach, the simulation of a whole textile sample usually required in mechanical characterization would lead to unfeasible calculation time. Therefore, a representative substructure is modelled using adequate boundary conditions to reproduce the behavior of the whole sample. The manufacturing process of multiaxial NCFs is a continuous process [30] in which the stitching process leads to a periodic network of the stitching yarns. Depending on the stitching pattern, the knitting cycle repeats exemplarily after each cycle (pillar pattern), two cycles (tricot pattern) or four cycles (tricot-chain pattern). In this study, the textile is modelled with a Representative Volume Element (RVE) based on the periodicity of the stitching pattern. The smallest RVE, defined as the smallest repetitive unit cell of the stitching yarn network, is referred to as the "elementary RVE". The size of the RVE can be derived from repetitions of the elementary RVE and denoted $r_W \times r_L$, where r_W and r_L correspond to the amount of repetitions perpendicular to the machine direction and in machine direction, respectively.

After introduction of the variability, the generated digital chains do not exhibit any periodicity at the edge of the RVE. Therefore, appropriate boundary conditions must be applied on the fibrous layer to ensure the representativeness of the model for a continuous textile. The implementation of symmetric boundary conditions would enable a free movement of the chains at the boundary causing their non-physical rearrangement. On the

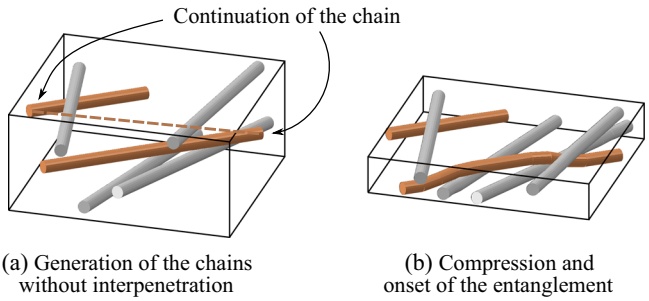

Fig. 4 Resolution of the interpenetration in fibrous layers including variability in the filament orientation

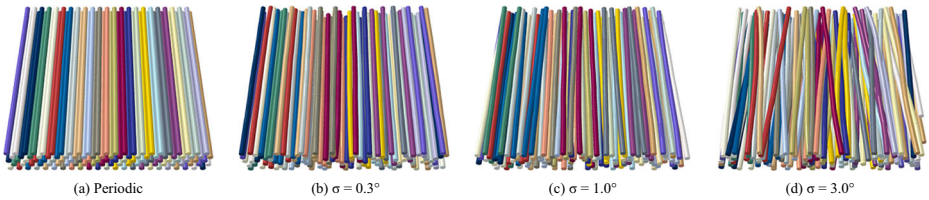

Fig. 5 Fibrous layers homogeneously generated without variability of the filament orientation (a) and with normally distributed filament orientations featuring standard deviations up to 3.0° (b) to (d)

contrary, fixing the transverse displacement of the end nodes would add an artificial transverse stiffness and would not be able to represent the onset of larger defects, such as gaps in a 0°-layer. Therefore, the authors propose the implementation of averaged periodic boundary conditions. To that end, a discretization of the RVE with a regular rectangular mesh is introduced at its boundaries, as illustrated in Fig. 6. Reference Points (RPs) are subsequently defined in the middle of each mesh element. The end nodes of the digital chains located in each mesh element are connected to the corresponding RP with averaged displacement boundary conditions as follows:

$$u_{RP} = \sum_{i=1}^{n} \frac{u_i}{n} \tag{2}$$

Where u_{RP} represents the displacement of the reference point, u_i the displacement of node i, and n the total amount of nodes in the mesh element.

Since the mesh of the RPs is regular, usual periodic boundary conditions can be applied on the RPs. Thereby, the displacement of periodic nodes, i.e. nodes at corresponding positions on opposed cross sections, are constrained to be equal. The size of the mesh elements is an important parameter of the model and is calculated to ensure that – on average – one end-node is located in a mesh element. This approach is selected to enable a direct comparison with a purely periodic material, which reduces in this case to the application of usual periodic boundary conditions. If no end-node is located in a mesh element, the element is progressively merged with the closest non-empty element. Thereby, the size of the mesh elements may change but still remains periodic. Moreover, contact surfaces are introduced at all faces of the volume boundary to model the fictive neighboring material and restrain the chains within the modelled volume. Note that standard periodic boundary conditions are applied to the stitching yarn chains since the RVE size correlates with the periodicity of the pattern. Using this approach, the overall periodicity of the material is ensured while allowing relative movements of the digital chains within the RVE. Moreover, any global deformation of the RVE can be

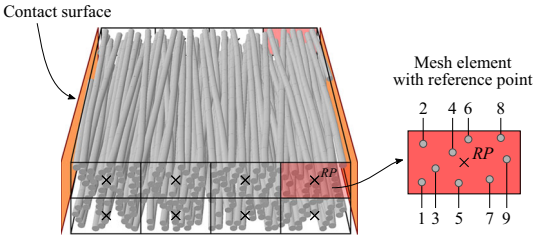

Fig. 6 Regular rectangular mesh defined at the boundary of the RVE with corresponding reference points (RPs) and contact surfaces (for better clarity, only the lateral surfaces are illustrated)

generated by applying relative displacements to the RPs and, thus, enables a virtual characterization of the material.

4.4 Stepwise Model Generation

The manufacturing process must be reproduced accurately in order to generate a realistic mechanical model of the "as-manufactured" geometry. In this work, it is proposed to simulate the piercing of the fibrous layers by the needles at all stitching points in a single step. Thereby, the digital chains are pushed apart when the needles penetrate the layers, as shown in Fig. 7(a) and 7(b). Subsequently, the stitching yarns are idealized using sharp edges at the location of piercing points (see Fig. 7(c)). Since the digital chains of the stitching yarn have no bending stiffness, the sharp geometries do not induce stress concentrations. The last simulation step consists of the pretension of the stitching yarn. To that end, a negative thermal load is applied to the stitching yarn chains to reproduce the tension induced by the knitting unit during the stitching process, as illustrated in Fig. 7(d). This approach allows for the reproduction of the defects induced during the stitching process and enables to account for manufacturing parameters (e.g. the tension in the stitching yarn) with reduced computational cost compared to a simulation of the whole stitching process. Moreover, the simulation approach is applicable using conventional contact algorithms and avoids potential numerical issues due to contact overclosure resolution.

4.5 Simulation Parameters

Due to the high amount of filaments in the textile, it is not possible to model each of them separately. Therefore, many filaments are grouped in a single digital chain. In order to generate comparable models with varying refinement level, the amount of filaments is first calculated based on the areal weight of each layer and on the density of the filaments. A packing coefficient is introduced as suggested in [31] to account for the packing of the filaments in the relaxed state. This numerical parameter can be approximated as a FVF in each chain. Finally, the refinement level and, thereby, the amount of digital chains is directly related to the chain diameter. In this study, the diameter of the DCE modelling the filaments is set to 69 μm, which represents a good compromise between calculation time and discretization level. With these parameters, each digital chain models about 49 filaments. It should be noted that the stiffness and the density of the chains are calculated depending on the packing coefficient and, thus, depending on the amount of filament grouped in the chains. Moreover, mass scaling is introduced in order to speed up the simulation. Table 3 summarizes the input parameters used for the numerical description of the NCFs. Although the stitching yarns are also constituted of many filaments, they are modeled with one single digital chain. According to [11], the actual diameter of the stitching yarn varies spatially due to the various compaction states of the yarns (i.e. compacted at the loops or flattened at the top surface). Nevertheless, a unique cross-section of the stitching yarn is assumed in the whole model, since the location of the chain elements may change during the application of the stitching yarn pretension. In order to model the stitching yarn at the region of inter-stitch interaction accurately, the diameter of the chain is calculated assuming a hexagonal packing (as suggested in [11]). The friction coefficients between the chains is set to a constant value of 0.3. It is representative for the values that can be found in studies focusing on the characterization of friction of carbon filaments at tow or filament level [32–34].

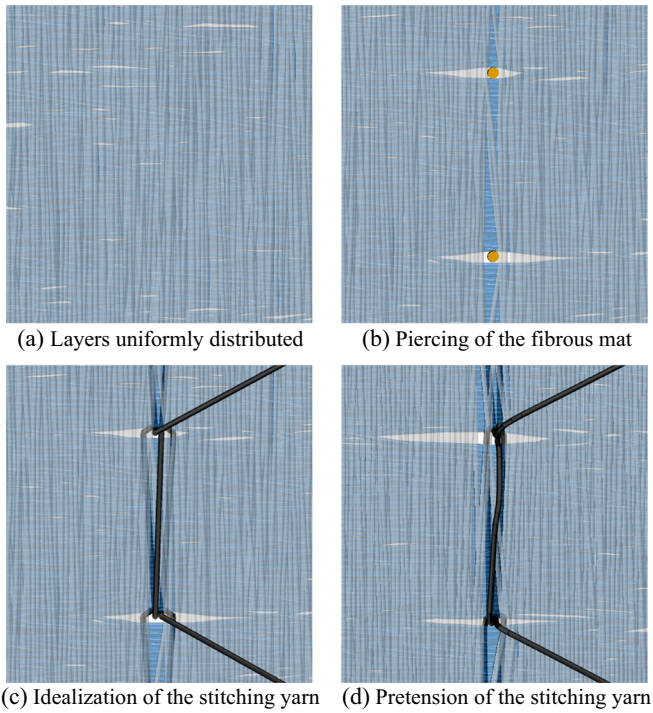

Fig. 7 Detailed view of the stepwise generation of the "as-manufactured" geometry

5 Results

5.1 Numerical Description of NCFs with Variability of the Filament Orientation

The two biaxial NCFs (0°/90° and ±45° NCFs) are considered in this section in order to show the ability of the approach to model various defects in the fibrous mat depending on the layer orientations and the standard deviation of the Gaussian distribution used to sample the orientation of the chains. First, various "as-manufactured" geometries of the 0°/90° NCF are illustrated in Fig. 8. The simulations are based on the parameters listed in Table 3 with different orientation variability in the layers (from a purely periodic fibrous mat up to a standard deviation of 3.0°). It can be determined that the purely periodic material (Fig. 8(a)) exhibit straight chains and that only channels are formed. With increasing variability (see Fig. 8(b) to 8(d)), the channels are progressively closing, starting from a few filaments crossing the channels and evolving to localized cracks. This correlates well with the conclusions drawn from the scans of the textile presented in section 3.1. Moreover, the onset of the gap over the whole length of the RVE shows the capability of the averaged periodic boundary condition to model local defects that propagate periodically beyond the RVE.

The numerical description of the ±45° NCF material is illustrated in Fig. 9, where local cracks can be observed at the stitching points and a waviness is induced in the chains orientation. This shows that the modelling approach is able to reproduce various types of defects already using the elementary RVE. A detailed comparison is proposed in the following subsections to assess the accuracy of the simulation approach.

5.2 Comparison of the Filament Orientations

The comparison of the simulation results with real samples is performed using larger models, namely 2 × 2 and 3 × 3 RVEs for the 0°/90° and ±45° NCF, respectively.

First, the chain orientation is compared with the measurements on the NCF material presented in section 3.1 to validate the modelling approach of the fibrous mat. In order to compare the final distribution of the chain orientation, the orientation of all DCEs is computed and projected on a 2D-plane parallel to the NCF. This enables a direct comparison with the measurements and is illustrated in Fig. 10. Since a random sampling of the chain orientation is used, the final orientation distribution of the numerical results is averaged from three independent calculations. The standard deviation of the Gaussian distributions used to generate the two "as-manufactured" geometries are listed in Table 3. A good agreement with the experimental distributions can be observed, which confirms the ability of the simulation approach to model a textile including realistic variability in the filament orientation. A further conclusion is that the standard deviation is a predominant input which can be used to model differences between two fibrous layers in a same NCF material. Nevertheless, slight differences have to be reported between the simulation results and measurements. For example, the distributions of the 0°/90° NCF are able to reproduce the peaks accurately, while small deviations occur for angles larger than 5 degrees. Further information on the filament orientation before the stitching process would increase the accuracy of the sampling distribution and, thus, the final distribution of the filament orientation.

5.3 Comparison of the Local Defects

A comparison of the local defects points out the ability of the approach to model various deviations induced by the stitching yarn. Using the reflection properties of the carbon filaments, it is possible to emphasize the defects in the NCFs as shown in Figs. 11 and 12.

As stated in section 3.2, a large variability of the defect size is observed in the fibrous layers. In the 0°/90° NCF, the type of defects of the "as-manufactured" geometry are well captured in the model (see Fig. 11). Channels are induced in the 0°-layer with filaments crossing from one tow to the neighboring one, while regular localized cracks are formed at the stitching points in the 90°-layer. On the front face of the ±45° NCF (i.e. 45°-layer) the

Table 3 Input parameters for the numerical description of the NCFs

		0°/90° NCF	±45° NCF
Filaments	Young's modulus [GPa]	120	127.5
	Density [g/cm^3]	0.905	0.890
	Diameter [μm]	69	69
	Packing coefficient [−]	0.5	0.5
	Mesh length [mm]	0.2	0.2
Fibrous layers	Layer thickness before stitching [mm]	0.41	0.43
	Standard deviation for the sampling [°]	1.15 (0°-layer)*	2.0 (+45°-layer)
		4.0 (90°-layer)*	2.0 (−45°-layer)
Stitching yarn	Young's Modulus [GPa]	1.81	1.81
	Density [g/cm^3]	1.25	1.25
	Diameter of the chains [μm]	88	71
	Mesh length [mm]	0.1	0.1
	Magnitude pretension [%]	16	17

*these parameters are not applicable to the simulations performed in section 5.1

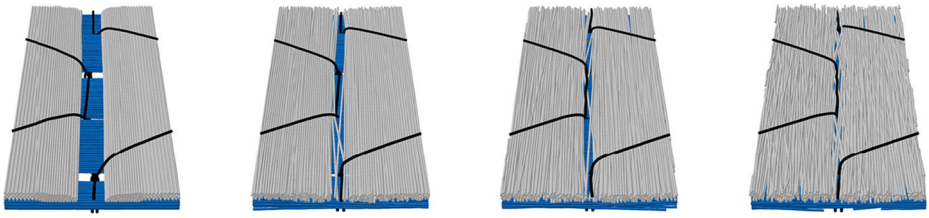

(a) Periodic (b) σ = 0.3° (c) σ = 1.0° (d) σ = 3.0°

Fig. 8 Elementary RVEs of the "as-manufactured" geometries of a 0°/90° biaxial NCF using purely periodic chains and with increasing standard deviation of the Gaussian sampling

same characteristics as those from real samples can be observed: at some stitching points almost no defects are noticeable while fish eye deformation with a length of several millimeters can be observed on the neighboring stitching point (ref. Figure 12(a)). On the contrary, the back face (i.e. −45°-layer) shows a regular formation of fish eye defects throughout the layer with various dimensions, as illustrated in Fig. 12(b).

The procedure presented in section 3.2 to measure the size of the defects was applied to the simulation results. The measured defect sizes are listed in Table 4 and a comparison between the experimental and numerical results is proposed in Fig. 13.

A good correlation of the mean values and their respective scatter can be observed. The size of the defects measured in the simulation of the ±45° NCF is slightly underestimated. Nevertheless, larger defects are generated in the −45°-layer than in the +45°-layer, an effect that corresponds to the experimental observations. Moreover, the cracks were not observable in the +45°-layer at 31% of the stitching points. This variability in the defect visibility correlates well with the ±45° NCF samples.

The defect length of the cracks generated in the 90°-layer is in complete agreement with the experimental data. In the 0°-layer, the width of the channels is underestimated while the scatter in the simulation results is significantly smaller than in experiments. It should be noted that the chain elements of the fibrous layers exhibit a diameter of 69 μm, which represents about 45% of the crack width in the ±45° NCF and 20% of the channel width of the 0°-layer. Thus, a single chain can have a considerable influence on the defect width and further refinement of the fibrous mat could increase the accuracy of the defect width. Also, the assumption of a tight packing in the chain elements of the stitching yarn throughout the model might lead to an underestimation of the defect size. Indeed, a reduced packing coefficient would yield larger stitching yarn and, thus, might increase the size of the defects. Finally, the angular tilt of the loops is measured in the simulation to 6.7° with a standard deviation of 3.1°. The numerical angular tilt is significantly smaller than in experiments (ca. 45% of the experimental values). Nevertheless, it shows that the simulation approach is able to capture deviations of the loop

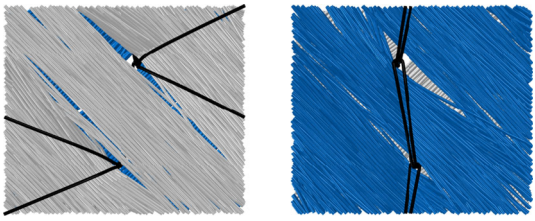

(a) Front face (b) Back face

Fig. 9 Elementary RVE of the "as-manufactured" geometry of the ±45° NCF

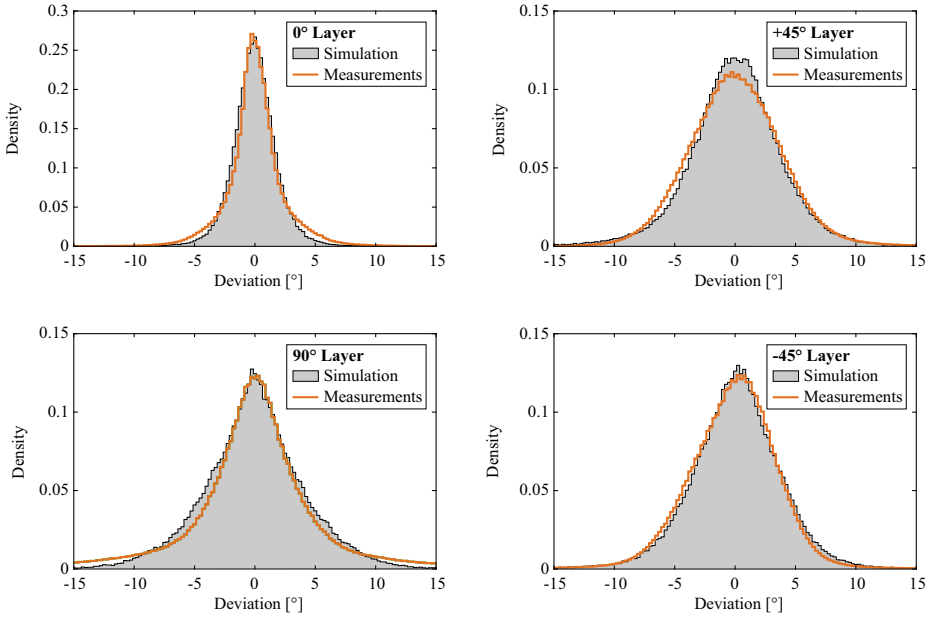

(a) 0°/90° NCF (b) ±45° NCF

Fig. 10 Comparison of the DCE orientation with the measurement on the samples of 0°/90° NCF (a) and ±45° NCF (b)

orientation from the theoretical alignment. It has been found that the magnitude of pretension of the stitching yarn influences the orientation of the loops, the size of the defects and thereby the orientation of the chains. Therefore, extended investigation on the pretension in the stitching yarn might be performed to improve the correlation.

The presented quantitative comparison validates the ability of the simulation to reproduce the local defects in the fibrous mat and the orientation variability of the filaments. Thus, the simulation approach proved its ability to generate a realistic numerical model of NCFs that can be used in further simulations.

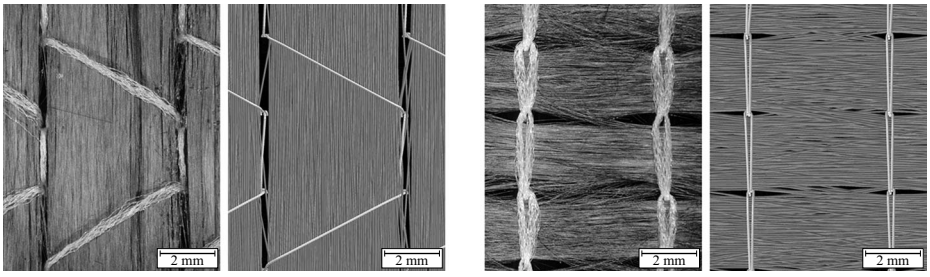

(a) Comparison of the 0°-Layer (b) Comparison of the 90°-Layer

Fig. 11 Comparison of the overall defect formation in the 0°-layer (a) and 90°-layer (b) between observations on the 0°/90° NCF samples (left) and simulation results (right)

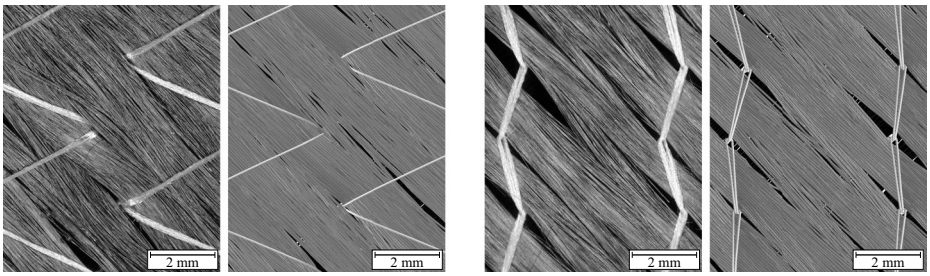

(a) Comparison of the 45°-Layer (b) Comparison of the -45°-Layer

Fig. 12 Comparison of the overall defect formation in the 45°-layer (a) and −45°-layer (b) between observations on the ±45° NCF samples (left) and simulation results (right)

6 Conclusion

A numerical mechanical description of dry non-crimp fabrics at the scale of the filaments was proposed. This method enables to describe a wide range of NCF architectures with realistic description of the local defects in the fibrous layers. Its applicability was demonstrated on two different configurations (0°/90° and ±45° biaxial NCFs). Variability in the filament orientation distribution was observed on two specimens and introduced in the simulation in order to model all interaction mechanisms within the textile (inter-filament, inter-stitch and stitch-to-filament interactions). A stepwise generation of the numerical "as-manufactured" geometry enabled the consideration of the main manufacturing steps and, thereby, the manufacturing process induced local defects in the fibrous mats. Averaged periodic boundary conditions have been developed to ensure an overall periodicity of the model while allowing reorientation of the chains at the smallest scale. Varying the orientation distribution in the model, a correlation has been found with the type of local defects induced at the stitching points. Also, the comparison of the filament orientation with the simulation results showed a good agreement and the detailed comparison of the local defects (cracks and channels) confirmed that the induced defects correlate with the experimental observations.

The presented approach is a mechanical description of the dry textile that includes all relevant interaction mechanisms. Hence, this framework can be easily integrated in the future in further simulations to predict the mechanical behavior of any NCF configuration (e.g. compaction or shear behavior) and, therefore, to study the influence of the stitching length, width or pattern on the deformation behavior. To that end, a calibration of the interaction parameters will be required to model the forces resulting from the respective interactions accurately. Moreover, the bending stiffness of the digital chains can be introduced in the framework if the forces resulting from bending deformation cannot be neglected compared to the axial forces of the chains and the

Table 4 Measured local defects on the simulation results

Designation	Layer	Defect type	Characteristic	Mean value [mm]	Standard deviation [mm]
0°/90° NCF	0°	channels	width	0,31	0,10
0°/90° NCF	90°	cracks	length	1,97	0,47
±45° NCF	45°	cracks	length	2,08	0,83
±45° NCF	45°	cracks	width	0,12	0,05
±45° NCF	−45°	cracks	length	2,62	1,13
±45° NCF	−45°	cracks	width	0,17	0,05

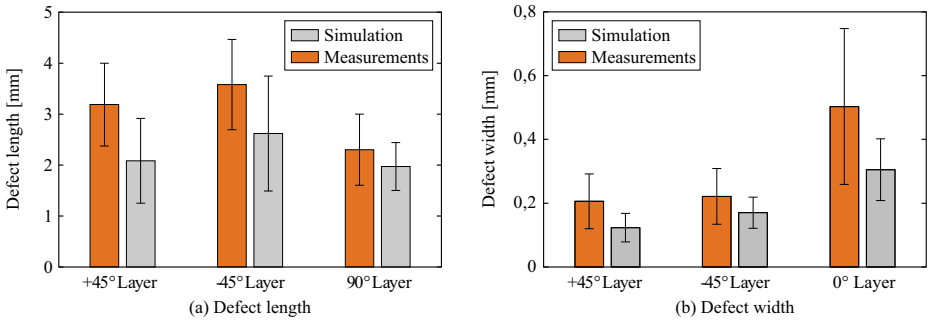

Fig. 13 Comparison of the defect width (a) and length (b) between the measurements performed on the NCFs samples and on simulation results (the error bars represent one pooled standard deviation)

interaction forces. In that case, the bending stiffness of the chains must be thoroughly studied to achieve a realistic deformation behavior depending on the amount of filaments modeled in each chain. Finally, the accurate description of the filament geometry at the refined scale can be used as input geometry for flow simulations in order to observe the influence of the local defects and orientation variability on the permeability of the textile.

Availability of Data and Material Not applicable.

Code Availability Not applicable.

Funding Information Open access funding provided by Projekt DEAL.

Compliance with Ethical Standards The authors declare that they have no conflict of interest.

Conflict of Interest The authors declare that they have no conflict of interest.

References

1. Lomov, S.V. (ed.): Non-Crimp Fabric Composites. Elsevier (2011)
2. Creech, G., Pickett, A.K.: Meso-modelling of non-crimp fabric composites for coupled drape and failure analysis. J. Mater. Sci. **41**(20), 6725–6736 (2006). https://doi.org/10.1007/s10853-006-0213-6
3. Wiggers, J.: Analysis of textile deformation during preforming for liquid composite moulding. Dissertation, University of Nottingham. http://eprints.nottingham.ac.uk/10414/ (2007)
4. Colin, D., Bel, S., Hans, T., Hartmann, M.: On the inter-stitch interaction in biaxial non-crimp fabrics. In: PROCEEDINGS OF THE 21ST INTERNATIONAL ESAFORM CONFERENCE ON MATERIAL FORMING: ESAFORM 2018, Palermo, Italy, 23–25 April 2018, p. 20004. Author(s) (2018). doi: https://doi.org/10.1063/1.5034805
5. Lomov, S.V., Barburski, M., Stoilova, T., Verpoest, I., Akkerman, R., Loendersloot, R., Thije, R.H.W.t.: Carbon composites based on multiaxial multiply stitched preforms. Part 3: Biaxial tension, picture frame

and compression tests of the preforms. Composites Part A: Applied Science and Manufacturing **36**(9), 1188–1206 (2005). doi: https://doi.org/10.1016/j.compositesa.2005.01.015
6. Krieger, H., Gries, T., Stapleton, S.E.: Design of Tailored non-Crimp Fabrics Based on stitching geometry. Appl. Compos. Mater. **38**(7), 1655–1127 (2017). https://doi.org/10.1007/s10443-017-9603-y
7. Chen, S., McGregor, O.P.L., Harper, L.T., Endruweit, A., Warrior, N.A.: Defect formation during preforming of a bi-axial non-crimp fabric with a pillar stitch pattern. Compos. A: Appl. Sci. Manuf. **91**, 156–167 (2016). https://doi.org/10.1016/j.compositesa.2016.09.016
8. Bel, S., Boisse, P., Dumont, F.: Analyses of the deformation mechanisms of non-crimp fabric composite reinforcements during preforming. Appl. Compos. Mater. **19**(3–4), 513–528 (2012). https://doi.org/10.1007/s10443-011-9207-x
9. Nguyen, N.Q., Mehdikhani, M., Straumit, I., Gorbatikh, L., Lessard, L., Lomov, S.V.: Micro-CT measurement of fibre misalignment. Application to carbon/epoxy laminates manufactured in autoclave and by vacuum assisted resin transfer moulding. Composites Part A: Applied Science and Manufacturing. **104**, 14–23 (2018). https://doi.org/10.1016/j.compositesa.2017.10.018
10. Fast, T., Scott, A.E., Bale, H.A., Cox, B.N.: Topological and Euclidean metrics reveal spatially nonuniform structure in the entanglement of stochastic fiber bundles. J. Mater. Sci. **50**(6), 2370–2398 (2015). https://doi.org/10.1007/s10853-014-8766-2
11. Lomov, S.V., Belov, E.B., Bischoff, T., Ghosh, S.B., Truong Chi, T., Verpoest, I.: Carbon composites based on multiaxial multiply stitched preforms. Part 1. Geometry of the preform. Composites Part A: Applied Science and Manufacturing **33**(9), 1171–1183 (2002). doi: https://doi.org/10.1016/S1359-835X(02)00090-8
12. Harrison, P., Yu, W.-R., Long, A.C.: Modelling the deformability of biaxial non-crimp fabric composites. In: Lomov, S.V. (ed.) Non-Crimp Fabric Composites, pp. 144–165. Elsevier (2011)
13. Boisse, P., Hamila, N., Vidal-Sallé, E., Dumont, F.: Simulation of wrinkling during textile composite reinforcement forming. Influence of tensile, in-plane shear and bending stiffnesses. Composites Science and Technology **71**(5), 683–692 (2011). doi: https://doi.org/10.1016/j.compscitech.2011.01.011
14. Yu, W.-R., Harrison, P., Long, A.: Finite element forming simulation for non-crimp fabrics using a non-orthogonal constitutive equation. Compos. A: Appl. Sci. Manuf. **36**(8), 1079–1093 (2005). https://doi.org/10.1016/j.compositesa.2005.01.007
15. Dumont, F., Weimer, C., Soulat, D., Launay, J., Chatel, S., Maison-Le-Poec, S.: Composites preforms simulations for helicopters parts. Int. J. Mater. Form. **1**(S1), 847–850 (2008). https://doi.org/10.1007/s12289-008-0268-9
16. Steer, Q., Colmars, J., Boisse, P.: Modeling of tricot stitch non crimp fabric in forming simulations. In: PROCEEDINGS OF THE 22ND INTERNATIONAL ESAFORM CONFERENCE ON MATERIAL FORMING: ESAFORM 2019, Vitoria-Gasteiz, Spain, 8–10 May 2019, p. 20004. AIP Publishing (2019). doi: https://doi.org/10.1063/1.5112509
17. Bel, S., Hamila, N., Boisse, P., Dumont, F.: Finite element model for NCF composite reinforcement preforming: importance of inter-ply sliding. Compos. A: Appl. Sci. Manuf. **43**(12), 2269–2277 (2012). https://doi.org/10.1016/j.compositesa.2012.08.005
18. Naouar, N., Vidal-Salle, E., Schneider, J., Maire, E., Boisse, P.: 3D composite reinforcement meso F.E. analyses based on X-ray computed tomography. Compos. Struct. **132**, 1094–1104 (2015). https://doi.org/10.1016/j.compstruct.2015.07.005
19. El Said, B., Green, S., Hallett, S.R.: Kinematic modelling of 3D woven fabric deformation for structural scale features. Compos. A: Appl. Sci. Manuf. **57**, 95–107 (2014). https://doi.org/10.1016/j.compositesa.2013.11.006
20. Sirtautas, J., Pickett, A.K., Lépicier, P.: A mesoscopic model for coupled drape-infusion simulation of biaxial non-crimp fabric. Compos. Part B. **47**, 48–57 (2013). https://doi.org/10.1016/j.compositesb.2012.09.088
21. Iwata, A., Inoue, T., Naouar, N., Boisse, P., Lomov, S.V.: Coupled meso-macro simulation of woven fabric local deformation during draping. Compos. A: Appl. Sci. Manuf. **118**, 267–280 (2019). https://doi.org/10.1016/j.compositesa.2019.01.004
22. Döbrich, O., Gereke, T., Cherif, C.: Modeling the mechanical properties of textile-reinforced composites with a near micro-scale approach. Compos. Struct. **135**, 1–7 (2016). https://doi.org/10.1016/j.compstruct.2015.09.010
23. Thompson, A.J., El Said, B., Belnoue, J.P.-H., Hallett, S.R.: Modelling process induced deformations in 0/90 non-crimp fabrics at the meso-scale. Compos. Sci. Technol. **168**, 104–110 (2018). https://doi.org/10.1016/j.compscitech.2018.08.029
24. Zhou, G., Sun, X., Wang, Y.: Multi-chain digital element analysis in textile mechanics. Compos. Sci. Technol. **64**(2), 239–244 (2004). https://doi.org/10.1016/S0266-3538(03)00258-6

25. Huang, L., Wang, Y., Miao, Y., Swenson, D., Ma, Y., Yen, C.-F.: Dynamic relaxation approach with periodic boundary conditions in determining the 3-D woven textile micro-geometry. Compos. Struct. **106**, 417–425 (2013). https://doi.org/10.1016/j.compstruct.2013.05.057
26. Durville, D.: Simulation of the mechanical behaviour of woven fabrics at the scale of fibers. Int. J. Mater. Form. **3**(S2), 1241–1251 (2010). https://doi.org/10.1007/s12289-009-0674-7
27. Moustaghfir, N., El-Ghezal Jeguirim, S., Durville, D., Fontaine, S., Wagner-Kocher, C.: Transverse compression behavior of textile rovings: finite element simulation and experimental study. J. Mater. Sci. **48**(1), 462–472 (2013). https://doi.org/10.1007/s10853-012-6760-0
28. Green, S.D., Long, A.C., El Said, B.S.F., Hallett, S.R.: Numerical modelling of 3D woven preform deformations. Compos. Struct. **108**, 747–756 (2014). https://doi.org/10.1016/j.compstruct.2013.10.015
29. Thumfart, S., Palfinger, W., Stöger, M., Eitzinger, C.: Accurate Fibre Orientation Measurement for Carbon Fibre Surfaces. In: Computer Analysis of Images, vol. 8048, pp. 75–82
30. Cherif, C. (ed.): Textile Materials for Lightweight Constructions. Technologies - methods - materials - properties. Springer, Heidelberg (2016)
31. Hans, T.N.: Finite element simulation of the braiding process. Dissertation, Technical University of Munich
32. Hans, T., Cichosz, J., Brand, M., Hinterhölzl, R.: Finite element simulation of the braiding process for arbitrary mandrel shapes. Compos. A: Appl. Sci. Manuf. **77**, 124–132 (2015). https://doi.org/10.1016/j.compositesa.2015.06.003
33. Vidal-Sallé, E., Massi, F.: Friction measurement on dry fabric for forming simulation of composite reinforcement. KEM 504-506, 319–324 (2012). doi: https://doi.org/10.4028/www.scientific.net/KEM.504-506.319
34. Cornelissen, B., Rietman, B., Akkerman, R.: Frictional behaviour of high performance fibrous tows. Friction experiments. Composites Part A: Applied Science and Manufacturing. **44**, 95–104 (2013). https://doi.org/10.1016/j.compositesa.2012.08.024